New Phytologist

Research

Arbuscular mycorrhizal fungi-indicative blumenol-C-glucosides predict lipid accumulations and fitness in plants grown without competitors

Yanrong You, Rishav Ray, Rayko Halitschke, Gundega Baldwin and Ian T. Baldwin

Department of Molecular Ecology, Max Planck Institute for Chemical Ecology, Jena 07745, Germany

Author for correspondence:
Ian T. Baldwin
Email: baldwin@ice.mpg.de

Received: *12 October 2022*
Accepted: *20 February 2023*

New Phytologist (2023) **238:** 2159–2174
doi: 10.1111/nph.18858

Key words: AMF-induced lipids, arbuscular mycorrhizal fungi, blumenol C-glucoside, *carotenoid cleavage dioxygenase 1* (*CCD1*), *Nicotiana attenuata*, plant fitness.

Summary

- Hydroxy- and carboxyblumenol C-glucosides specifically accumulate in roots and leaves of plants harboring arbuscular mycorrhizal fungi (AMF).
- To explore blumenol function in AMF relationships, we silenced an early key-gene in blumenol biosynthesis, *CCD1* (*carotenoid cleavage dioxygenase 1*), in the ecological model plant, *Nicotiana attenuata*, and analyzed whole-plant performance in comparison with control and *CCaMK*-silenced plants, unable to form AMF associations.
- Root blumenol accumulations reflected a plant's Darwinian fitness, as estimated by capsule production, and were positively correlated with AMF-specific lipid accumulations in roots, with relationships that changed as plants matured when grown without competitors. When grown with wild-type competitors, transformed plants with decreased photosynthetic capacity or increased carbon flux to roots had blumenol accumulations that predicted plant fitness and genotype trends in AMF-specific lipids, but had similar levels of AMF-specific lipids between competing plants, likely reflecting AMF-networks.
- We propose that when grown in isolation, blumenol accumulations reflect AMF-specific lipid allocations and plant fitness. When grown with competitors, blumenol accumulations predict fitness outcomes, but not the more complicated AMF-specific lipid accumulations. RNA-seq analysis provided candidates for the final biosynthetic steps of these AMF-indicative blumenol C-glucosides; abrogation of these steps will provide valuable tools for understanding blumenol function in this context-dependent mutualism.

Introduction

Arbuscular mycorrhizal fungal (AMF) symbioses are widespread associations between most land plants and a few fungal taxa of the subphylum Glomeromycotina (Smith & Read, 2008; Spatafora *et al.*, 2016). The plant provides the fungus with carbon in the form of lipids and sugars, while the fungus supplies the plant with mineral nutrients (predominantly P as Pi) captured from soil (Roth & Paszkowski, 2017). The AMF relationship is highly context-dependent, covering the entire spectrum of fitness outcomes for host plants, from parasitism to mutualism, depending on the environment, and may play a central role in many other poorly studied interactions among higher plants, in addition to its well-studied role in P-nutrition (Bennett & Groten, 2022). This context dependence is likely a reflection of the large (20% of net fixation, Bago *et al.*, 2000) C investments for the host plants and that AMF can exchange these investments among neighboring plants, even among different species (Figueiredo *et al.*, 2021).

During AMF symbiosis, many lipid biosynthetic and metabolism genes are upregulated, and AMF-specific lipid biosynthetic and transfer genes involved in fungal nourishment are known (Gaude *et al.*, 2012; Bravo *et al.*, 2016; Jiang *et al.*, 2017; Keymer *et al.*, 2017; Luginbuehl *et al.*, 2017). However, the regulation of photoassimilate transfer from aboveground parts to this resource-intensive belowground symbiosis remains elusive. Many studies have focused on whole-plant P signaling, as P is the best-studied mineral nutrient transported to host plants by AMF, and is a major regulator of the symbiosis (Johnson *et al.*, 2010; Nouri *et al.*, 2014). Recent advances reveal that a phosphate starvation response-centered network regulates mycorrhizal symbiosis (Shi *et al.*, 2021; Das *et al.*, 2022). In addition, phytohormones, microRNAs, and secreted peptides all regulate and integrate the development of AMF relationships in concert with host plant P status (Müller & Harrison, 2019; Nouri *et al.*, 2021). Recent research in apocarotenoids has identified several groups of new signaling molecules (Moreno *et al.*, 2021). For example, zaxinones regulate strigolactone (SL) and abscisic acid (ABA) biosynthesis in Arabidopsis roots (Ablazov *et al.*, 2020) and regulate growth and AMF colonization levels in rice (Wang *et al.*, 2019; Votta *et al.*, 2022); blumenol-C-glycosides accumulate in the aboveground parts of most AMF-harboring plants in proportion to AMF arbuscule number and health (Wang *et al.*, 2018a).

Here, we explore the latter of these new apocarotenoid signals in the AMF–host plant relationship.

Blumenols are C-13 cyclohexenone derivatives, produced by the cleavage of C-40 carotenoids and are classified into three major types: blumenol A, blumenol B, and blumenol C. Only the blumenol C glycosides are positively correlated with AMF relationships. Studies in the native tobacco, *Nicotiana attenuata*, identified two blumenol C glycosides (11-hydroxyblumenol C-9-O-Glc and 11-carboxyblumenol C-9-O-Glc) as the first quantitative shoot markers for AMF relationships (Wang *et al.*, 2018a). These two compounds were discovered through a sophisticated unbiased metabolomics comparison between AMF-harboring wild-type (WT) plants and plants transformed to silence the *calcium- and calmodulin-dependent protein kinase* (ir*CCaMK*; ir: inverted repeat) that is essential for the establishment of the symbiosis (Groten *et al.*, 2015). The two blumenols specifically accumulate in roots after AMF inoculation and are transferred to shoots in levels that positively correlate with root colonization rates (Wang *et al.*, 2018a). However, the biological function of these blumenol markers that accumulate in the shoots in all AMF-harboring species studied to date (Wang *et al.*, 2018a) remains unknown. Here, we explore their potential whole-plant signaling function in the plant–AMF relationship.

The first committed step in blumenol biosynthesis, engages carotenoid cleavage dioxygenases (CCDs), an evolutionarily conserved family of nonheme Fe^{2+}-dependent enzymes, which catalyzes double bond-specific cleavage reactions of carotenoids and apocarotenoids (Floss *et al.*, 2008; Fiorilli *et al.*, 2019). Carotenoid cleavage dioxygenase 1 (CCD1) can cleave several carotenoid and apocarotenoid substrates at different positions along the carbon backbone (Felemban *et al.*, 2019), and studies in *Medicago truncatula* demonstrated that CCD1 uses a C-27 apocarotenoid as the major substrate, and is involved in the production of blumenols in AMF-colonized root cells (Floss *et al.*, 2008). After AMF colonization, a C-40 carotenoid is cleaved by CCD7 to produce a C-13 cyclohexenone and a C-27 apocarotenoid, which is subsequently cleaved again by CCD1 to yield a second C-13 cyclohexenone (Floss *et al.*, 2008). As the subsequent enzymes that form the hydroxyl- and carboxyblumenol C-glucosides from the C-13 cyclohexenone (likely P450s and glycosyltransferases, respectively) are unknown, we focused on silencing by RNA interference (RNAi) the specific alleles of *CCD1* in *N. attenuata* that are transcriptionally regulated by AMF interactions. Not only is CCD1 a committed step in blumenol biosynthesis, silencing its expression in *M. truncatula* is known to alter arbuscule development and turnover (Floss *et al.*, 2008), providing tantalizing hints that these blumenols may function as whole-plant signals in the AMF relationship.

Previous research with *N. attenuata* revealed that plants silenced in the expression of *GAL83*, a β-subunit of a heterotrimeric SnRK1 (SNF1-related kinase) kinase complex, by antisense (as) RNAi (as*GAL83*), had constitutively increased allocations of recently fixed carbon to roots (Schwachtje *et al.*, 2006). Another study revealed that silencing *ribulose-1,5-bisphosphate carboxylase/oxygenase (RuBPC) activase* using an inverted repeat (ir) construct (ir*RCA*), increased the concentrations of inactive RuPBC protein, decreasing photosynthetic capacity and whole-plant carbon allocation to roots (Mitra & Baldwin, 2008). Here, we used these two RNAi lines as genetic tools to manipulate C-flux to roots. Additionally, we also generated new RNAi-silenced transgenic plants (ir*CCD1*) in which the AMF-induced alleles of *NaCCD1* (a/b but not c/d) in roots were strongly silenced to investigate the biological function of blumenols. As RNAi in these homozygous lines is sufficiently strong to function in hemizygous states, we crossed the ir*CCD1* lines with the as*GAL83* and ir*RCA* lines to interrogate the plant–AMF–blumenol relationship by genetically perturbing whole-plant carbon allocation patterns.

As we were interested in the whole-plant fitness consequences of AMF relationships, and since *N. attenuata* is a self-fertilizing annual plant, we used seed set as a relevant proxy for its fitness. As seed number per capsule, seed mass, viability, and dormancy of selfed seeds show only minor variations as a function of location along the inflorescence (Baldwin & Morse, 1994; Euler & Baldwin, 1996; Baldwin *et al.*, 1997, 1998), we used lifetime capsule production as a proxy for Darwinian fitness. As this native tobacco is a fire-chasing plant that germinates synchronously from long-lived seedbanks after fires in the Great Basin Desert (Baldwin & Morse, 1994; Baldwin *et al.*, 1994), relative growth rates are very important in determining fitness outcomes, and we have developed a two-plant/pot competitive growth system that facilitates the quantification of fitness differences that reflect differences in growth rates (Glawe *et al.*, 2003).

We performed RNA-seq analysis of empty vector (EV), ir*CCaMK*, and ir*CCD1* plants with or without AMF symbiosis to identify the biological pathways induced by AMF and those correlated with blumenol accumulations. As the lipid sector was highly regulated by AMF, we analyzed the fitness and the blumenol–lipid relationships of EV, ir*CCaMK*, and ir*CCD1* plants grown without competitors in 1-l pots, harvested at three developmental stages. Blumenol accumulations correlated strongly with lipid and fitness differences. As fitness relationships are robustly quantified in plants under competitive growth, we grew ir*CCD1* and two isogenic lines with reduced C-fixation (ir*RCA*) and increased C-partitioning to roots (as*GAL83*) and their hemizygous crosses and quantified fitness and blumenol–lipid relationships. Surprisingly, while blumenols predicted fitness outcomes, lipid concentrations were similar between competing plants in the same pot. As ir*CCD1* plants have reduced blumenol levels and altered arbuscule maturation patterns (Floss *et al.*, 2008), we reanalyzed the co-variance of the RNA-seq data with blumenol levels to identify candidate enzymes involved in the last steps of the blumenol biosynthesis amongst the differentially regulated glucosyltransferases (GSTs) and cytochrome P450s (CYPs) that could catalyze the later-stage hydroxylation/carboxylation/glycosylation steps. We predict that plants silenced in one of these terminal steps could provide valuable tools for understanding the potential signaling functions of blumenols.

Materials and Methods

Plant materials and growth conditions

An inbred line (31st generation) of *Nicotiana attenuata* Torr. Ex Watts was used as the WT genetic background for all

transformants. Previously described homozygous plants of the T3 generation of the ir*CCaMK* line (A-09-12121-4; Groten *et al.*, 2015) and the empty vector control line (EV, A-03-266-3-7; Bubner *et al.*, 2006) were used in this study.

NaCCD1a/b-silenced lines were produced by the published *Agrobacterium tumefaciens*-mediated transformation method (Krügel *et al.*, 2002) using a pSOL8 binary transformation vector (Gase *et al.*, 2011) containing an inverted repeat (ir) fragment of the *NaCCD1a* (*NIATv7_g18324*) and *NaCCD1b* (*NIATv7_g18325*) sequences. The primers used for the construct are listed in Supporting Information Table S1. The transgenic lines were screened following the procedures described previously (Gase *et al.*, 2011). The number of insertion copies and the fidelity of the insertions (over-reads and truncations) were evaluated by NanoString nCounter® analysis (He *et al.*, 2019). The T3 generation of two individual diploid, homozygous transgenic lines (ir*CCD1*_45#: A-18-045-1-4 and ir*CCD1*_48#: A-18-048-7-3) were used in this study.

Hybrid plants were generated by crossing the previously characterized transgenic lines ir*RCA* (A-03-462-7; Mitra & Baldwin, 2008) and as*GAL83* (A-263-3-4; Schwachtje *et al.*, 2006) with EV (A-03-266-3), ir*CCD1*_45# (A-18-045-1) and ir*CCD1*_48# (A-18-048-7) lines, and the F1 seeds were used in this study.

For glasshouse experiments, seeds were germinated on Gamborg B5 medium as previously described (Krügel *et al.*, 2002), and the inoculation experiments were performed as previously described (Wang *et al.*, 2018a; Song *et al.*, 2019). In brief, seedlings were transferred into dead (autoclaved twice at 121°C for 30 min; noninoculated controls) or living inoculum (*Rhizophagus irregularis*, Biomyc Vital, AMF-inoculated plants) diluted 1 : 10 with expanded clay (size: 2–4 mm). Plants were watered every second day with a hydroponic fertilizer solution with 1/10 of the regular inorganic Pi content (for 1 l regular hydroponic fertilizer solution: 0.1292 g $CaSO_4 \times 2H_2O$, 0.1232 g $MgSO_4 \times 7H_2O$, 0.0479 g K_2HPO_4, 0.0306 g KH_2PO_4, 2 ml KNO_3 (1 M), 0.5 ml micronutrients, 0.5 ml Fe diethylene triamine pentaacetic acid) for 2 wk (50 ml per plant for plants in the rosette stage of growth), and then with a hydroponic fertilizer solution with 1/4 Pi concentration when the plants entered the elongation stage (100 ml per plant). Plants were grown separately in 1-l pots (non-competitive; diameter 13 cm × 11 cm) or two plants of different genotypes grown together in 2-l pots (competitive; diameter 14 cm × 15 cm). Plants were maintained under standard glasshouse conditions (16 h : 8 h, 24–28°C : 20–24°C, light : dark, and 45–55% humidity). During harvests, roots were carefully washed, briefly dried with a paper towel, cut into 1-cm pieces, and mixed. An aliquot was stored in root storage solution (99% ethanol and 60% acetic acid, 3 : 1, v/v) and stored at 4°C for microscopic analysis. The remaining root material, as well as stem leaves from identical developmental stages, was immediately frozen in liquid nitrogen and stored at −80°C for further analyses (Wang *et al.*, 2018a).

For the field experiments, seeds were imported and released under APHIS notification numbers 07-341-101n (EV), 18-282-102m (ir*CCD1*). Seeds were soaked for 1 h in 5 ml liquid smoke (House of Herbs Inc., Passaic, NJ, USA) solution, ×50 diluted in water and supplemented with 50 µl of 0.1 M gibberellic acid, GA3 (Roth, Karlsruhe, Germany). Then, the seeds were planted directly into a field plot at the Lytle Ranch Preserve in the Great Basin Desert (lat. 37.145580°, long. −114.021150°). At harvest, the roots of the plants were carefully excavated, and washed with water. Fine roots were harvested and wrapped in aluminum foil, shipped to the laboratory on dry ice and stored at −80°C for further analyses.

Plant fitness estimates

The total capsule number of each plant was counted at 9 wk post inoculation (wpi) with or without colonization before harvest. Mean (± SD) capsule numbers of 11 plants (Fig. 2e) and eight plants (Fig. 5e,h) of each genotype and treatment were counted.

Root staining and colonization assessment

Trypan blue staining was performed as previously described (Song *et al.*, 2019). In brief, roots were cleared with 20% KOH (96°C, 5 min), and acidified with 2% HCl (96°C, 5 min), and then stained with a 0.05% Trypan blue solution (lactic acid : glycerol : distilled water (1 : 1 : 1, v/v); 96°C, 3 min) and mounted on a microscope slide. Root AMF colonization was evaluated using the method described previously (Wang *et al.*, 2018a). Briefly, >150 view-fields per slide were surveyed with a ×20 magnification of a regular optical microscope and classified into five groups: no colonization (N), only hyphae (H), hyphae with arbuscules (H + A), hyphae with arbuscules and vesicles (H + A + V), and hyphae with vesicles (H + V). The percentages of each group were calculated by the number of each sector divided by total views.

WGA-Alexa Fluor 488 staining was performed as previously described (Jiang *et al.*, 2017). Roots were placed in 50% ethanol for >4 h and then transferred to 20% (w/v) KOH for 2–3 d, followed by 0.1 M HCl for 1–2 h at room temperature. After HCl was removed, the sample was rinsed twice with distilled H_2O, and once with 1× phosphate-buffered saline buffer, and then immersed in PBS/WGA-Alexa Fluor 488 staining solution (0.2 µg ml^{-1}) in the dark for 6 h. Root length colonization was imaged under a Zeiss confocal microscope (LSM 510 META; Zeiss, Jena, Germany).

Extraction and analysis of blumenol markers, ABA, and lipids

Plant samples were ground in liquid nitrogen to a fine powder and *c.* 100 mg tissue was aliquoted for extractions. Blumenol markers and ABA were extracted and analyzed according to Wang *et al.* (2018a). In brief, 100 mg of plant tissue was extracted using 800 µl of 80% MeOH containing 10 ng stable isotope-labeled abscisic acid (D_6-ABA; HPC Standards GmbH, Borsdorf, Germany) as an internal standard. After centrifugation, the supernatant was collected and analyzed. Five microliters of the blumenol extracts was injected into an UHPLC (Dionex

UltiMate 3000, Thermo Fisher Scientific, Waltham, MA, USA) equipped with a reversed phase column (Agilent Zorbax Eclipse XDB C18; 50 mm × 3.0 mm, 1.8 µm; Agilent Technologies, Santa Clara, USA). Analytes were eluted at a flow rate of 0.5 ml min^{-1} and a column oven temperature of 42°C with a binary gradient system consisting of solvent A (0.05% HCOOH and 0.1% acetonitrile in water) and solvent B (MeOH). The elution gradient was as follows: 0–1 min, 10% B; 1–1.2 min, 10–35% B; 1.2–3 min, 35–42% B; 3–3.4 min, 42–100% B; 3.4–4.4 min, 100% B; 4.4–4.5 min, 100–10% B and 4.5–5.5 min, 10% B. Compounds were quantified with specific MRMs on a Bruker Elite EvoQ triple quadrupole MS equipped with a heated electrospray ionization (HESI) ion source as described previously (Wang *et al.*, 2018a).

Lipids were extracted and analyzed as previously described (Salem *et al.*, 2016). Briefly, 100 mg of plant tissue was homogenized in 1 ml of extraction solvent A (methyl tertiary-butyl ether : MeOH, 3 : 1, v/v) in a GenoGrinder 2000 (SPEX SamplePrep, Metuchen, NJ, USA) for 60 s at 1000 strokes min^{-1} using two 4-mm steel balls (Askubal, Korntal-Münchingen, Germany). To each sample, 2 µg of 1,3-18:0 D5-DG (800855P; Avanti Polar Lipids Inc., Alabaster, AL, USA) and 2 µg of 16:0-18:0-16:0 D5-TG (860902P; Avanti Polar Lipids Inc.) were added as internal standards. Then, the samples were incubated on an orbital shaker at 100 rpm for 45 min at 4°C and sonicated for 15 min in an ice-cooled sonication bath. After the sonication, 650 µl of solvent B (H_2O : MeOH, 3 : 1, v/v) were added to the sample tube, and mixed by vortexing for 1 min. After centrifugation at a speed of 15 000 ***g*** for 5 min at 4°C, 400 µl of the solvent from the upper, lipid-containing phase was collected and evaporated using a nitrogen flow evaporator, dissolved in 400 µl solvent C (acetonitrile : MeOH, 7 : 3, v/v), and analyzed by LC–MS. Two microliters of the lipid extracts was injected into an UltiMate 3000 UHPLC system (Thermo Fisher Scientific, Waltham, MA, USA) equipped with a Phenomenex Kinetex C8 column (50 mm × 2.0 mm, 2.6 µm particle size). Analytes were eluted at a flow rate of 0.4 ml min^{-1} and a column oven temperature of 25°C with a binary gradient system consisting of solvent A (10 mM ammonium acetate and 0.1% acetic acid in water) and solvent B (10 mM ammonium acetate and 0.1% acetic acid in acetonitrile : isopropanol, 7 : 3, v/v). The elution gradient was as follows: 0–0.5 min, 40% B; 0.5–10.0 min, 40–70% B; 10.0–37.5 min, 70–100% B; 37.5–40.0 min, 100% B, after which the column was equilibrated at the initial conditions for 4 min. The lipids were detected on a time-of-flight mass spectrometer (microTOF; Bruker, Billerica, MA, USA) operating in positive electrospray ionization mode (capillary voltage: 4500 V, dry temperature: 200°C, dry gas: 10 l min^{-1}, nebulizer gas: 1.6 bar). Mass spectra were recorded with a mass range of *m/z* 50–1400, and the mass spectrometer was calibrated before each sample run using sodium formate. DAG and TAG signals were annotated based on the exact mass of their molecular ion and characteristic neutral losses indicating the chain length and degree of unsaturation of the fatty acid groups. The intensity of the $[M + NH_4]^+$ ammonium adduct was used to quantify the lipids.

Statistical analysis

Statistical analysis of the data was made in GraphPad Prism 9.1.0. For analysis of differences between two groups of data, Student's *t*-tests were used with the two-tailed distribution of two sets of samples with equal variance. Different statistical significance between multiple groups (≥ 3) of data was evaluated using analysis of variance (ANOVA), followed by Tukey's or Šídák's multiple comparisons tests recommended by the software.

Methods for phylogeny analysis, reverse transcription-qPCR (RT-qPCR), RNA sequencing, *in vitro* enzymatic activity assays, and gene accession numbers are listed in Methods S1.

Results

To investigate the biological functions of blumenol markers in plant–AMF relationships, we first characterized *CCD1* in *N. attenuata*. By blasting the homologues of *MtCCD1* (Floss *et al.*, 2008), *SlCCD1* (Simkin *et al.*, 2004), *AtCCD1* (Schwartz *et al.*, 2001), *OsCCD1* (Ko *et al.*, 2018), and *ZmCCD1* (Sun *et al.*, 2008), we identified four genes, *NaCCD1a*, *NaCCD1b*, *NaCCD1c*, and *NaCCD1d*, in the *N. attenuata* genome. A molecular phylogenetic analysis revealed that the NaCCD1a and NaCCD1b proteins were closely related to SlCCD1 and MtCCD1 (Fig. S1a). Gene expression analysis revealed that *NaCCD1a* and *NaCCD1b* transcripts are highly induced in EV (an isogenic transgenic line transformed with an empty vector transformation construct) plants after AMF colonization by *R. irregularis* (Fig. S1b). This AMF-elicited increase in transcript abundance was abolished in ir*CCaMK* plants that did not establish AMF symbiosis (Fig. S1b), consistent with the accumulation of blumenol markers (Wang *et al.*, 2018a). However, the transcripts of the other *CCD1* genes, *CCD1c* and *CCD1d*, showed no clear associations with AMF. From these results, we infer that *NaCCD1a* and *NaCCD1b* are mainly involved in the AMF-induced blumenol biosynthesis. We next generated several stable transgenic lines expressing an RNAi construct, which silenced both *NaCCD1a* and *NaCCD1b* with two inverted repeat tandem repeats (Fig. S1c,d). Two independent homozygous transgenic lines, ir*CCD1*_45# and ir*CCD1*_48#, each harboring single, complete insertions without read-throughs or truncations (Fig. S1e), were selected for further research. *CCD1a* and *CCD1b* expression was silenced in these two lines, with or without AMF colonization (Fig. 1a), while the expression of the other two homologous genes, *CCD1c* and *CCD1d*, were unaffected.

To evaluate the utility of these lines for tests of blumenol function, we compared their blumenol levels with those of EV as positive, and ir*CCaMK* plants as negative controls for the AMF interaction. Blumenol levels were significantly reduced in the roots of these two ir*CCD1* lines at both the early (4 wpi) and later stages (9 wpi) of the AMF-interaction (Fig. 1b), consistent with the role of CCD1 in the blumenol biosynthesis. Blumenol levels were also reduced in leaf samples of the ir*CCD1* lines at 9 wpi (Fig. 1c). We also planted EV and ir*CCD1*_45# in their native habitat, the Great Basin Desert in North America, and found that

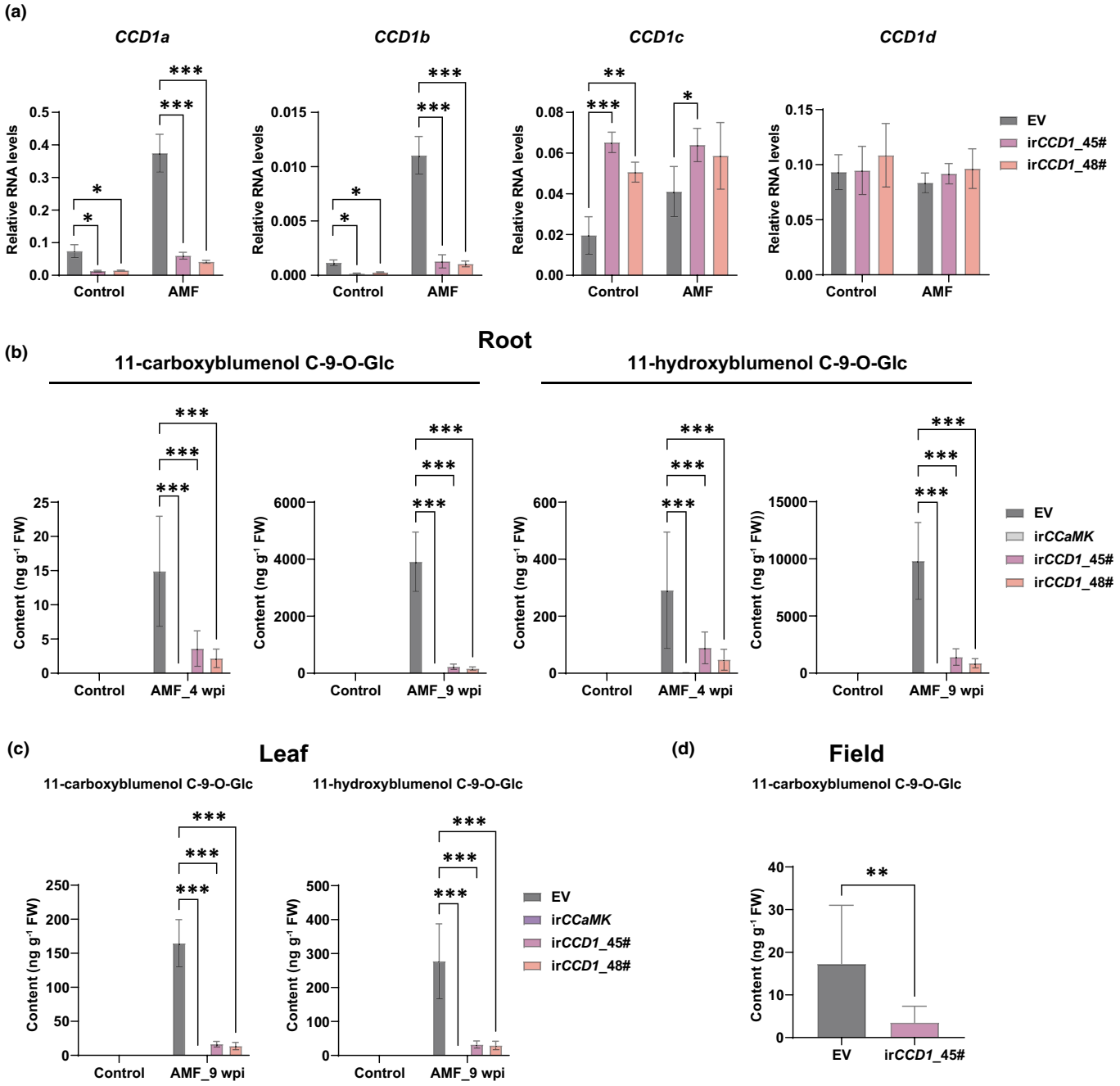

Fig. 1 Inverted repeat *carotenoid cleavage dioxygenase 1* (ir*CCD1*) plants have reduced blumenol accumulations. (a) Transcript abundance of four *NaCCD1* genes in root samples of empty vector (EV) and two independent ir*CCD1* transgenic lines inoculated with or without (control) *Rhizophagus irregularis*. Mean ± SD, $n = 4$. (b) Abundances of 11-carboxyblumenol C-9-O-Glc and 11-hydroxyblumenol C-9-O-Glc in root samples of EV, inverted repeat *calcium- and calmodulin-dependent protein kinase* (ir*CCaMK*), and ir*CCD1* plants (at 4 and 9 wk post inoculation (wpi)) inoculated with or without (control) *R. irregularis*. Mean ± SD, $n = 8$. (c) 11-carboxyblumenol C-9-O-Glc and 11-hydroxyblumenol C-9-O-Glc concentrations in leaf samples of EV, ir*CCaMK*, and ir*CCD1* plants inoculated with (at 9 wpi) or without (control) *R. irregularis*. Mean ± SD, $n = 8$. (a–c) Two-way analysis of variance with Tukey's multiple comparisons test. Asterisks indicate significant differences between the means: *, $P < 0.05$; **, $P < 0.01$; ***, $P < 0.001$. If no asterisks are given, means were not significantly different. (d) 11-carboxyblumenol C-9-O-Glc concentrations in root samples of EV and ir*CCD1* plants grown at the Utah field station. Mean ± SD, $n = 10$; Student's *t*-test: **, $P < 0.01$.

the blumenol levels were also reduced in field-grown ir*CCD1* plants, revealing that *CCD1* silencing robustly truncates blumenol accumulations in complex natural environments with native AMF taxa.

CCD1 affects AMF colonization and plant fitness

To investigate the effects of reduced blumenol accumulations in ir*CCD1* plants, we analyzed the transcript levels of AMF-induced

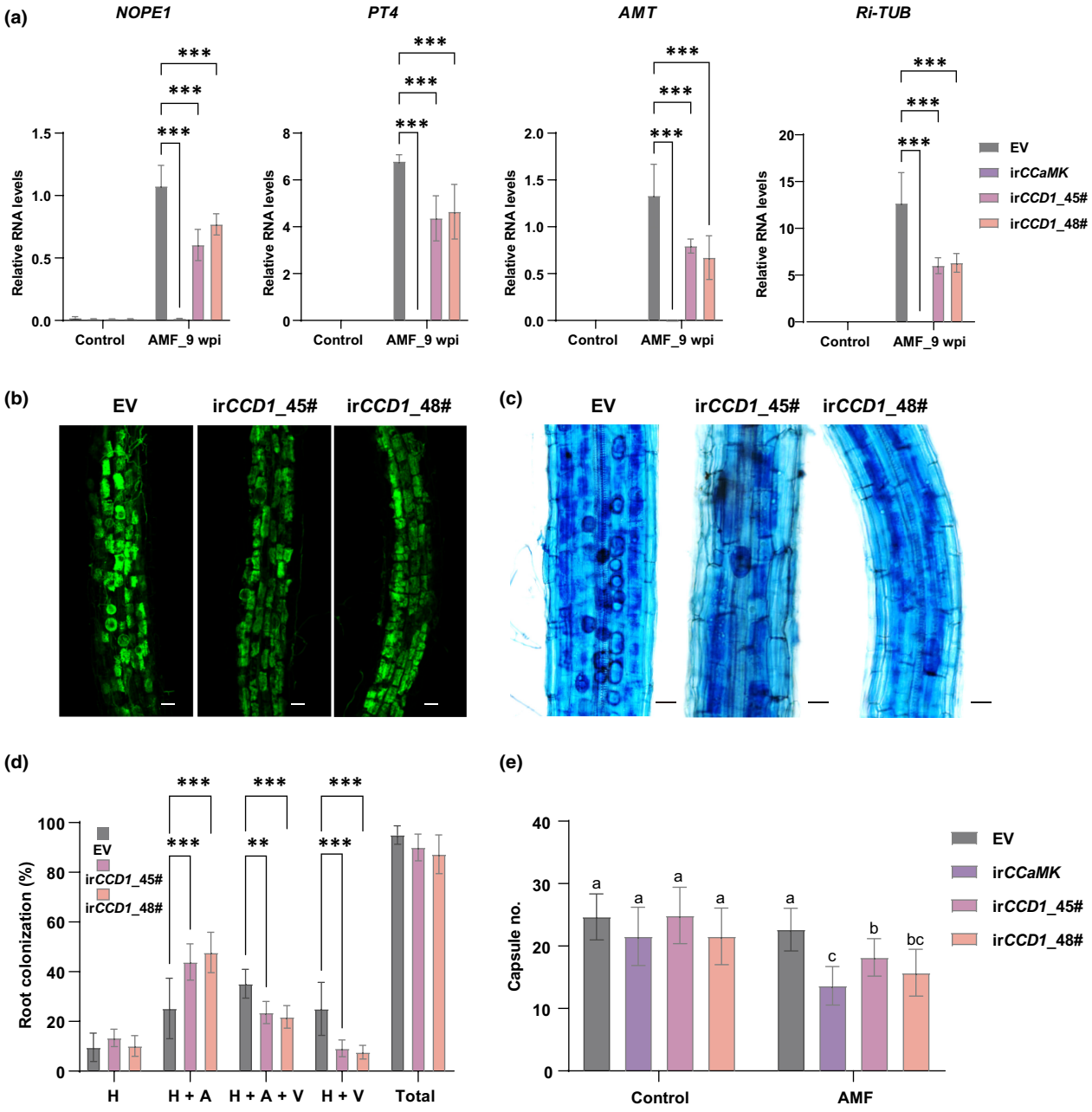

Fig. 2 Inverted repeat *carotenoid cleavage dioxygenase 1* (ir*CCD1*) plants are impaired in arbuscular mycorrhizal fungi (AMF) colonization and fitness. (a) Transcript abundance of classical arbuscular mycorrhizal symbiosis-marker genes in roots of empty vector (EV), inverted repeat *calcium- and calmodulin-dependent protein kinase* (ir*CCaMK*), and ir*CCD1* plants inoculated with or without *Rhizophagus irregularis*. Mean ± SD, $n = 4$. (b) Representative confocal microscopy images of WGA-Alexa Fluor 488 stained roots of EV and ir*CCD1* plants inoculated with *R. irregularis* (9 wk post inoculation (wpi)). Bars, 50 μm. (c) Representative images of trypan blue stained roots of EV and ir*CCD1* plants inoculated with *R. irregularis* (9 wpi). Bars, 50 μm. (d) Colonization analysis of roots of EV and ir*CCD1* plants. A, arbuscules; H, hyphae; Total, total root length colonization; V, vesicles. Mean ± SD, $n = 8$. (e) Capsule numbers analysis of EV, ir*CCaMK*, and ir*CCD1* plants inoculated with (9 wpi) or without (control) *R. irregularis*. Mean ± SD, $n = 11$. (a, d, e) Two-way analysis of variance with Tukey's multiple comparisons test: (a, d) **, $P < 0.01$; ***, $P < 0.001$; (e) different letters indicate significant differences between the columns, $P < 0.05$.

marker genes in roots of EV, ir*CCaMK*, and the two ir*CCD1* lines in plants grown with or without AMF. RT-qPCR results showed that transcript accumulations of *NOPE1*, an identified *N*-acetylglucosamine transporter required for AMF symbiosis in rice and maize (Nadal *et al.*, 2017); the phosphate transporter *PT4* (Javot *et al.*, 2007), as well as the ammonium transporter *AMT* (Breuillin-Sessoms *et al.*, 2015), were all reduced in ir*CCD1* lines compared with EV plants (Fig. 2a) and were not detected in ir*CCaMK* plants. In addition, the expression of *R. irregularis TUBULIN* (*Ri-TUB*), a specific housekeeping gene of *R. irregularis*, was also reduced in ir*CCD1* plants (Fig. 2a), indicating that ir*CCD1* attenuates AMF colonization.

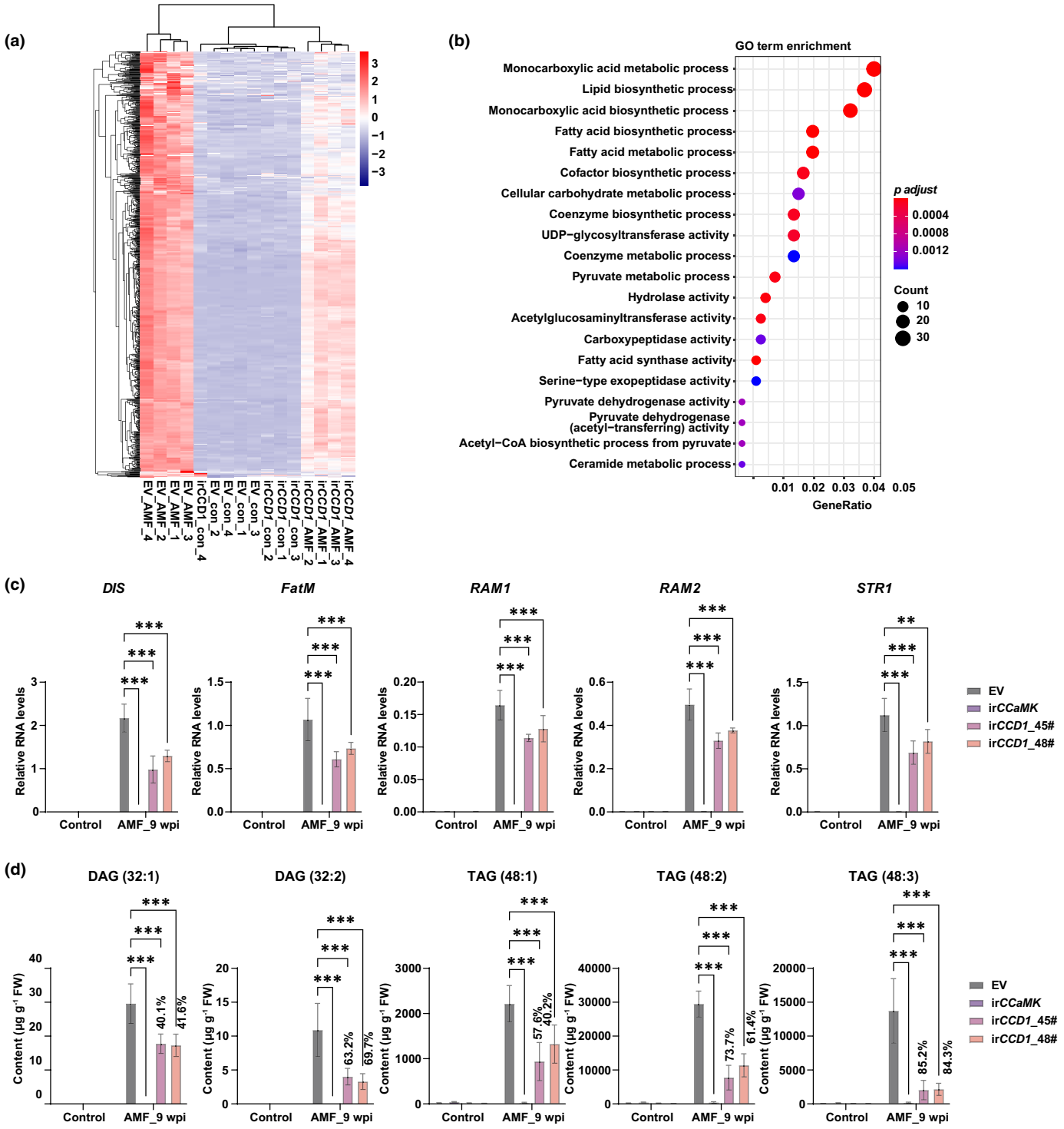

Fig. 3 Arbuscular mycorrhizal fungi (AMF)-induced lipid biosynthesis is decreased in inverted repeat *carotenoid cleavage dioxygenase 1* (ir*CCD1*) plants. (a) Transcriptome analysis of roots of empty vector (EV) and ir*CCD1* plants inoculated with (AMF) or without (Con) *Rhizophagus irregularis*. Heat map showing expression levels of 853 AMF-induced genes that require CCD1 for their induction. (b) Gene ontology (GO) enrichment analysis of the 853 genes in (a). (c) Transcript abundance of AMF-induced fatty acid and lipid biosynthesis genes in roots of EV, inverted repeat *calcium- and calmodulin-dependent protein kinase* (ir*CCaMK*), and ir*CCD1* plants inoculated with (9 wk post inoculation (wpi)) or without (control) *R. irregularis*. Mean ± SD, $n = 4$. (d) Concentrations of AMF-induced lipids DAG 32:1 (16:1,16:0), DAG 32:2 (16:1. 16:1), TAG 48:1 (16:1, 16:0, 16:0), TAG 48:2 (16:1, 16:1, 16:0) and TAG 48:3 (16:1, 16:1, 16:1) in roots of EV, ir*CCaMK*, and ir*CCD1* plants inoculated with (9 wpi) or without (control) *R. irregularis*. Percentage numbers are the rate of decrease in ir*CCD1* lines. Mean ± SD, $n = 10$. (c, d) Two-way analysis of variance with Tukey's multiple comparisons test: **, $P < 0.01$; ***, $P < 0.001$.

To more thoroughly characterize the altered AMF relationships, we conducted microscopic quantifications of WGA-Alexa Fluor 488- and trypan blue-stained roots of EV and ir*CCD1* plants (Fig. 2b). Arbuscules are highly branched, tree-shaped hyphal structures that form in root cortical cells and which are known to be the site of AMF-host plant nutrient exchange (Gutjahr & Parniske, 2013). While we did not observe the same changes in the arbuscular structure as has been reported in *CCD1*-silenced *Medicago* (Floss *et al.*, 2008), we found that arbuscules were much more abundant in ir*CCD1* roots compared with those of EV roots (Fig. 2b); while the vesicles, the lipid storage structures (Choi *et al.*, 2018), were decreased in ir*CCD1* lines (Fig. 2c). The statistical analysis of root colonization patterns confirmed these impressions, with increased arbuscules and decreased vesicles in ir*CCD1* lines (Fig. 2d), indicating that silencing *CCD1* influences the AMF colonization.

We estimated plant fitness from lifetime total capsule numbers of EV, ir*CCaMK*, and ir*CCD1* lines with and without AMF and found that the overall fitness of AMF-harboring lines was not significantly improved over AMF-free plants under the glasshouse growth conditions of low P regimes, as previous studies had shown (Riedel *et al.*, 2008). However, when only comparing AMF-inoculated plants, the fitness benefits of the AMF were clear: Capsule numbers of ir*CCD1* lines were significantly reduced than those of EV plants, and the numbers were further reduced in ir*CCaMK* plants (Fig. 2e), patterns which reflected the plants' AMF-induced blumenol levels (Fig. 1b).

ir*CCD1* influences AMF-induced lipid biosynthesis

Since *NaCCD1a/b* silencing influences AMF colonization and plant fitness, we used RNA-seq to compare the transcriptomes of roots of EV, ir*CCaMK*, and ir*CCD1* plants with or without AMF to further identify the biological pathways induced by AMF and those correlated with blumenol accumulations. PCA of transcript abundances revealed that the AMF-colonized and control samples were clearly distinct, and the four biological replicates of the different genotypes clustered well (Fig. S2a). We identified 2435 genes that were upregulated by AMF in the roots of EV plants and 2502 genes with significantly reduced transcript abundances in ir*CCD1* roots compared with EV plants after AMF colonization. Comparison of these two sets of genes led to the identification of 853 genes with reduced transcript levels in AMF-colonized ir*CCD1* roots, which are upregulated in AMF-colonized EV roots (Fig. S2b; Dataset S1-1). The expression patterns of this larger dataset are shown in a heat map analysis (Fig. 3a; Dataset S1-1). Gene ontology (GO) analysis and GO network analysis revealed that genes of the fatty acid and lipid biosynthesis pathways were enriched (Figs 3b, S2c; Dataset S1-2, 3). RT-qPCR analysis further confirmed that the transcript levels of well-known lipid biosynthesis genes *DISORGANIZED ARBUSCULES* (*DIS*), *Mycorrhizal acyl-ACP thioesterase* (*FatM*), *Reduced Arbuscular Mycorrhiza 1* (*RAM1*), *Required for Arbuscular Mycorrhization 2* (*RAM2*), as well as the ABC transporter gene *STUNTED ARBUSCULE 1* (*STR1*), which are induced by AMF (Keymer & Gutjahr, 2018), were all significantly reduced in ir*CCD1* lines compared with those of EV plants, and their transcripts were not detected in ir*CCaMK* plants (Fig. 3c). From these results, we infer that AMF-specific lipid biosynthesis, which is essential for the fungal growth, is strongly downregulated in ir*CCD1* plants. We tested this inference by lipid analysis.

To analyze the lipid profiles of the roots of EV, ir*CCaMK*, and the two ir*CCD1* lines with or without AMF colonization, we employed untargeted liquid chromatography coupled with time of flight mass spectrometry (LC-TOF-MS) analyses. *Rhizophagus irregularis* is known to accumulate large quantities of nonpolar storage lipids, triacylglycerols (TAG), and these storage lipids are found in lipid particles in the cytosol of fungal cells, mainly in extraradical spores and intraradical vesicles (Bago *et al.*, 2000; Wewer *et al.*, 2014). We found that the levels of DAG 32:1 (16:1, 16:0), DAG 32:2 (16:1, 16:1), TAG 48:1 (16:1, 16:0, 16:0), TAG 48:2 (16:1, 16:1, 16:0), and TAG 48:3 (16:1, 16:1, 16:1) were highly increased in AMF-colonized roots of EV plants (Fig. 3d), consistent with previous studies (Wewer *et al.*, 2014; Bravo *et al.*, 2017). By contrast, the AMF induction of these lipids was abolished in the roots of ir*CCaMK* plants, and substantially truncated in the roots of ir*CCD1* plants (Fig. 3d). Taken together, we conclude that AMF-induced lipid biosynthesis is impaired in the ir*CCD1* plants.

In addition, we also analyzed the lipids in field-grown EV and ir*CCD1* plants and found that the lipids of DAG 32:1, TAG 48:1, TAG 48:2, TAG 48:3 were also reduced significantly in ir*CCD1* plants than those of EV plants (Fig. S3), consistent with the blumenol level (Fig. 1d), revealing that *CCD1* silencing also attenuates lipid biosynthesis in plants colonized by native AMF taxa.

Plant hormones ABA and SL are derived from the same carotenoid biosynthetic pathway as blumenols and have also been reported to be involved in mycorrhization (Herrera-Medina *et al.*, 2007; Hou *et al.*, 2016; Felemban *et al.*, 2019; Moreno *et al.*, 2021). To test whether silencing *CCD1* influences the biosynthesis of these two apocarotenoid phytohormones, we analyzed the expression level of *CCD7* and *CCD8*, the well-known SL biosynthesis genes (Felemban *et al.*, 2019; Li *et al.*, 2020), in ir*CCD1* plants. We found no difference between EV and ir*CCD1* plants in the abundance of *CCD7* and *CCD8* transcripts at basal level without AMF colonization, but transcript levels decreased in ir*CCD1*_45#, but not in ir*CCD1*_48# plants compared with the EV plants after AMF colonization (Fig. S4a,b). As the AMF-related phenotypes in ir*CCD1*_45# and ir*CCD1*_48# plants are similar, we excluded the effect of expression differences of *CCD7* and *CCD8* as being important for the phenotypes of ir*CCD1* plants. In addition, we also measured the ABA levels in the ir*CCD1* plants, and found that silencing *CCD1* did not influence ABA level (Fig. S4c,d).

Blumenol levels are positively correlated with AMF-induced lipids

As the lipids levels (Fig. 3d) track the blumenol accumulation patterns (Fig. 1b) in the roots of EV, ir*CCaMK*, and ir*CCD1* plants, we conducted correlational analyses among blumenols

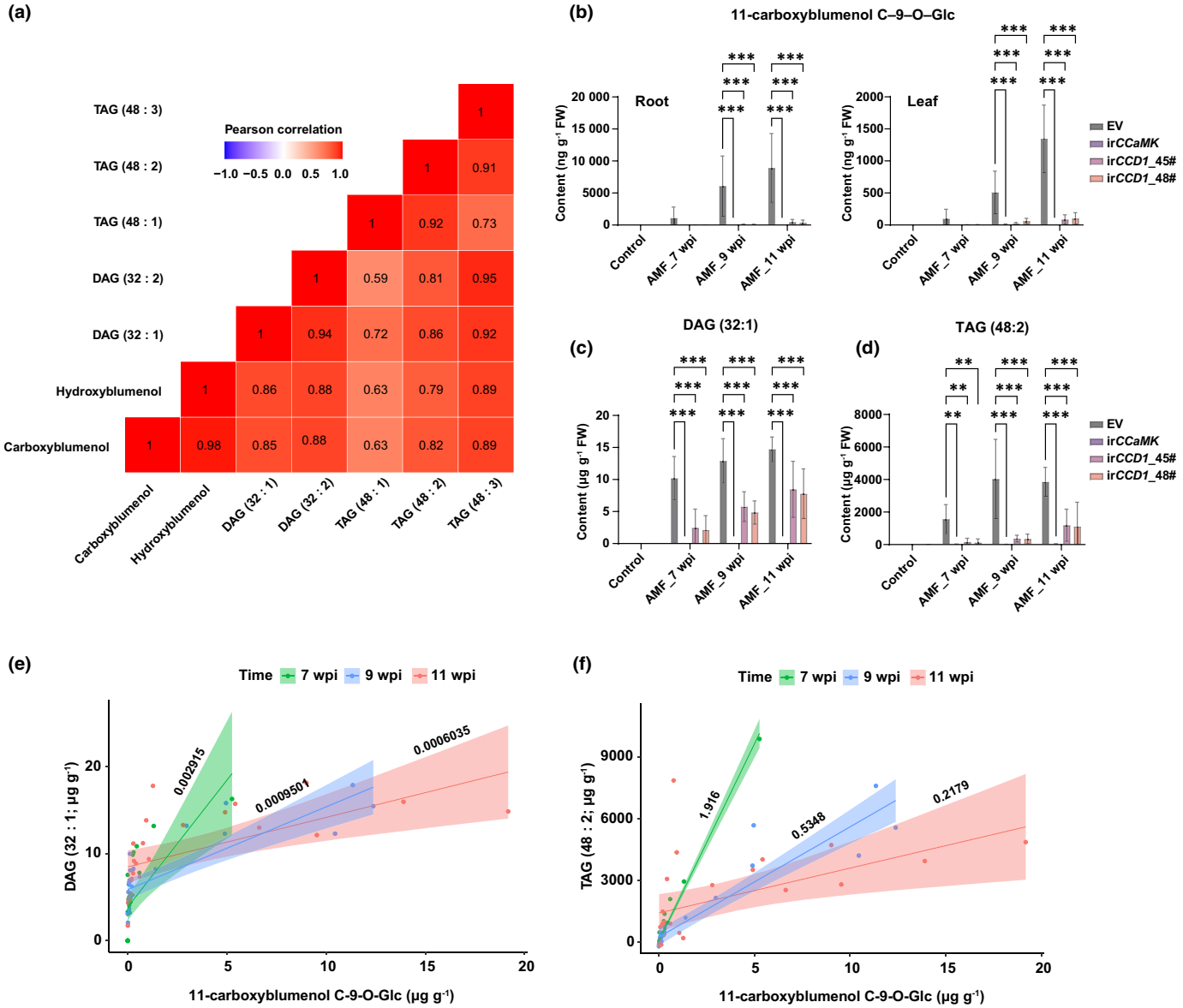

Fig. 4 Blumenols are positively correlated with arbuscular mycorrhizal fungi (AMF)-induced lipids in singly-grown plants. (a) Pearson correlation analysis of root blumenol (shown in Fig. 1b) and lipid concentrations (shown in Fig. 3d) of empty vector (EV) and ir*CCD1* plants. (b) 11-carboxyblumenol C-9-O-Glc concentrations in root and leaf samples of EV, inverted repeat *calcium- and calmodulin-dependent protein kinase* (ir*CCaMK*), and inverted repeat *carotenoid cleavage dioxygenase 1* (ir*CCD1*) plants (at 7, 9, and 11 wk post inoculation (wpi)) inoculated with or without (control) *Rhizophagus irregularis*. Mean ± SD, $n = 8$. (c, d) AMF-induced lipids, DAG 32:1 (c) and TAG 48:2 (d), in roots of EV, ir*CCaMK*, and ir*CCD1* plants (at 7, 9, and 11 wpi) inoculated with or without (control) *R. irregularis*. Mean ± SD, $n = 8$. (b–d) Two-way analysis of variance with Tukey's multiple comparisons test: **, $P < 0.01$; ***, $P < 0.001$. (e) Covariance analyses of 11-carboxyblumenol C-9-O-Glc (shown in Fig. 4b, left panel) and DAG 32:1 (shown in Fig. 4c) in roots of the EV and ir*CCD1* plants. (f) Covariance analyses of 11-carboxyblumenol C-9-O-Glc (shown in Fig. 4b, left panel) and TAG 48:2 (shown in Fig. 4d) in roots of the EV and ir*CCD1* plants. (e, f) The numbers are the slopes of simple linear regression and the colored zones reflect 95% confidence intervals.

and lipids during the development of the host plant–AMF association. Pearson's correlation analysis between root blumenols (Fig. 1b, 9 wpi) and lipids (Fig. 3d) of the EV and ir*CCD1* plants revealed that both carboxyblumenol and hydroxyblumenol markers were highly and positively correlated with all lipids identified as specifically induced in AMF-colonized roots (Fig. 4a).

In contrast to the blumenol markers that are known to accumulate without significant turnover in shoot tissues (Wang *et al.*, 2018a), a plant's lipid allocation to AMF would be expected to wane as plants fill and mature seed capsules to realize their fitness and senesce arbuscules. To examine the inference that the blumenol–lipid relationships would change over plant ontogeny, we performed a time–course analysis of AMF-inoculated plants grown in individual pots. We harvested roots and leaf samples of EV, ir*CCaMK*, and the two ir*CCD1* lines at three times that span the reproduction–senescence transition for glasshouse-grown plants and analyzed the blumenol and lipid levels: at 7, 9, and 11 wpi. As the two blumenols have the same

accumulation patterns in glasshouse-grown plants (Fig. 1b,c), and similar lipid relationships (Fig. 4a), we used the carboxyblumenol and DAG 32:1 and TAG 48:2 as examples of how the blumenol–lipid relationship changes over ontogeny. As shown in Fig. 4b, blumenols, both in roots and in leaves of the EV plants, increased during reproductive maturation, albeit at much lower levels in the ir*CCD1* plants. The lipids showed a similar accumulation pattern with the blumenols at the early stage (Figs 4c,d, S5a), but the rate of increase at the later stages became slower. Consistent with this, the covariance analysis showed that the slopes of the positive correlations between blumenols and lipids decreased as the plants matured (Figs 4e,f, S5b–d).

Blumenol levels predict plant fitness both in competitive and noncompetitive environments

As *c.* 20% of plant photoassimilates are transferred to AMF in the form of carbohydrates and lipids (Bago *et al.*, 2000; Jiang *et al.*, 2017), we used the ir*RCA* line, which reduces whole-plant C-fixation, and the as*GAL83* line, which increases C-partitioning to roots, to manipulate C-flux to roots (Fig. 5a). We crossed ir*CCD1*_45# and 48# plants with these two lines, and as fitness relationships are robustly quantified in plants under competitive growth, we grew EV and the two ir*CCD1* lines and their hemizygous crosses with the isogenic ir*RCA* and as*GAL83* lines in 2-l pots (Fig. 5b). The blumenol accumulations were reduced in all lines with the ir*CCD1* background compared with the EV background after AMF colonization (Figs 5c,f, S6a,c). Consistent with the blumenol levels, capsule numbers were also reduced in all lines with ir*CCD1* background compared with EV plants after AMF colonization (Fig. 5e,h). Interestingly, unlike the blumenol and fitness pattern, there were no differences in the root lipid composition between plants with EV or ir*CCD1* background in the same pots (Figs 5d,g, S6b,d). However, the amounts of accumulated lipids decreased in the order predicted by the background genotype's allocation of C to roots (e.g. as*GAL83* > EV > ir*RCA*). We hypothesize that plants grown in competition in the same pot share the same common mycorrhizal networks (CMNs) and that lipids are distributed within the fungal hyphal network connecting different plant roots. This hypothesis could be tested with a number of different experimental approaches including both physical (Song *et al.*, 2019) and genetic means (as carried out in this study using ir*CCaMK* plants) to uncouple plants from the CMNs (Groten *et al.*, 2015; Wang *et al.*, 2018a,b), but another promising approach would be to specifically abrogate blumenol biosynthesis.

Identifying candidate enzymes involved in blumenol biosynthesis

Although ir*CCD1* plants have reduced blumenol levels and are useful tools to investigate the biological functions of the blumenol markers, plants abrogated in the final biosynthetic steps of these AMF-specific blumenol C-glucosides would provide more valuable tools, because other functionally important but uncharacterized apocarotenoids may also be changed when silencing *CCD1*. Based on the accumulation pattern of blumenols in EV, ir*CCaMK*, and ir*CCD1* (Fig. 1b), we reanalyzed the RNA-seq data and found a set of genes that are highly induced by AMF in roots of EV plants, showed no response in ir*CCaMK* plants, and had intermediate levels of expression in ir*CCD1* plants (Figs 6a, S7a; Dataset S2-1). Among this gene set, several *glucosyltransferases* (*GSTs*) and *cytochrome P450s* (*CYPs*) were identified, which might be involved in the last catalytic steps of the two AMF-specific blumenol C-glucosides, including the glycosylation or the hydroxylation/carboxylation reactions (Fig. 6b,c; Dataset S2-2). Using a chemically deglycosylated product of byzantionoside B (the isomer of blumenol C glucoside; Fig. S7b) as the most closely related, commercially available substrate, we identified one *GST* gene, *GST4*, which is likely involved in the glycosylation of the blumenol markers (Fig. S7c). Further assays should be done to confirm the function of GST4 in the blumenol biosynthesis, and also identify the *CYPs* involved in the hydroxylation/carboxylation steps. Once these last blumenol–biosynthetic steps are uncovered, the generation of knockdown or knockout transgenic lines silenced in one of these terminal steps could provide valuable tools for understanding the potential signaling functions of blumenols, and for the identification of other factors that influence the highly context-dependent plant–AMF relationships.

Discussion

Hydroxy- and carboxyblumenol C-glucosides accumulate specifically in roots colonized by AMF. We silenced the expression of *CCD1*, an early and committed gene in blumenol biosynthesis to reduce blumenol accumulation during AMF colonization to investigate the biological function of blumenols. We found that blumenols are highly and positively correlated with AMF-induced lipid accumulation when plants were grown in noncompetitive environments and the relationship changes as plants mature. In addition, blumenols also predict plant fitness both in both competitive and noncompetitive environments. However, two observations from this work deserve further discussion: that the AMF-relationship for plants grown in pots in the glasshouse resulted in fitness decreases (Fig. 5e,h), and that no differences were found in the lipid levels of plants sharing the same pot (Figs 5d,g, S6b,d).

Our data showed that the fitness of plants was reduced after inoculation with AMF compared with autoclaved inoculum (Fig. 5e,h). This phenomenon of mycorrhizal-induced growth depression has been observed and discussed by many others (Johnson *et al.*, 1997; Lendenmann *et al.*, 2011; Jin *et al.*, 2017). As plants need to allocate photosynthetic carbon below ground for transfer to the symbiotic partner, the fungi might be considered to be parasitic on plants when the demands for organic carbon (C) from the host plant outweigh any benefits that might be gained from P transfers via the fungus (Johnson *et al.*, 1997). Many abiotic factors including soil nutrients, pH, water, and light availability also influence the effectiveness of AMF ranging from mutualistic to parasitic (Ronsheim, 2012; Groten *et al.*, 2015; Jin *et al.*, 2017). In addition, biotic factors such as

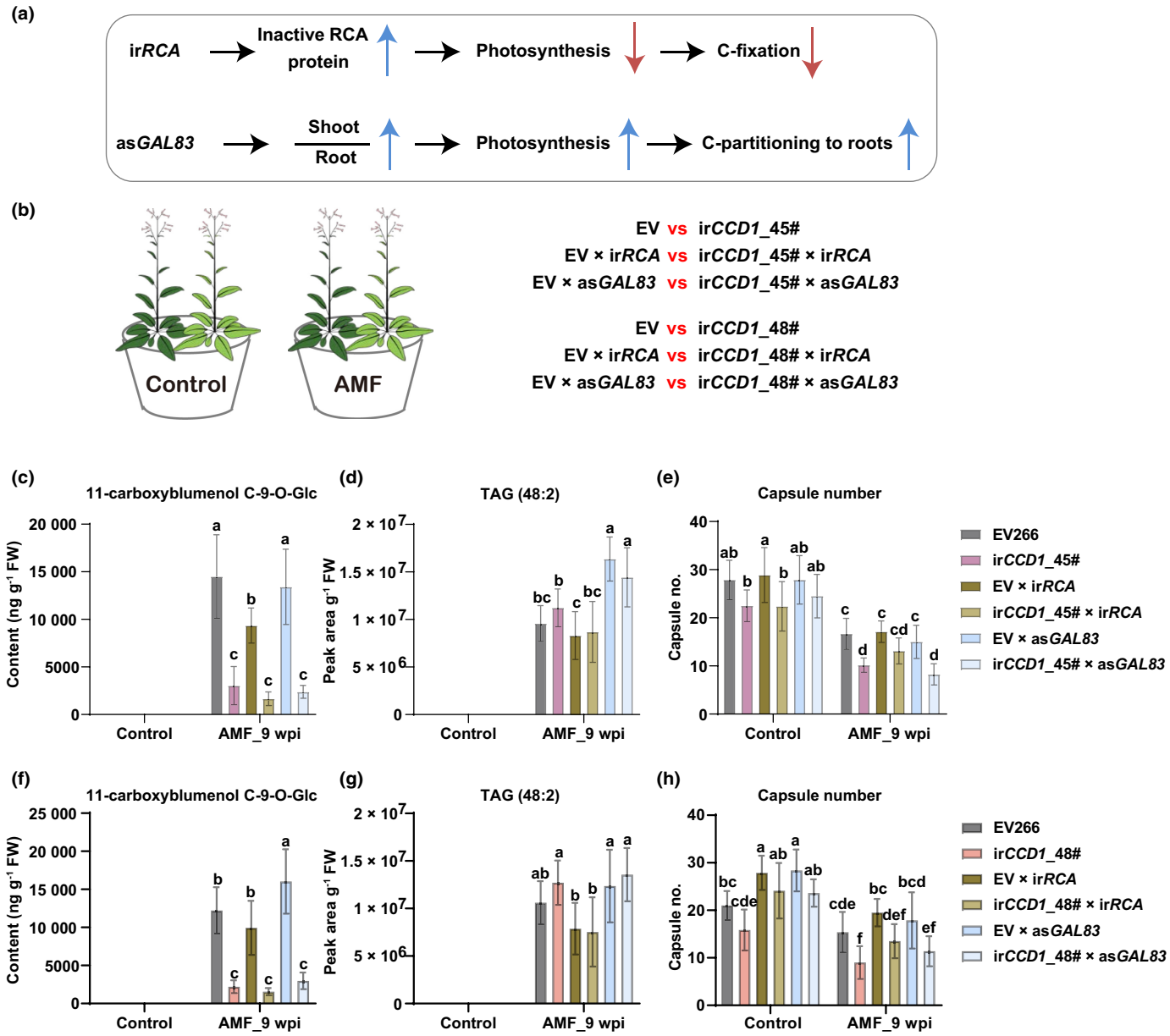

Fig. 5 Blumenols predict plant fitness in competitive environments. (a) Schematic diagram of root–shoot C-flux relationships in inverted repeat *construct* (ir*RCA*) and as*GAL83* transgenic plants. The blue arrows indicate increases, and red arrows indicate decreases. (b) Schematic of crossings and paired-plantings in 2-l pots. (c, d) Concentrations of 11-carboxyblumenol C-9-O-Glc (c) and arbuscular mycorrhizal fungi (AMF)-induced lipid TAG 48:2 (d) in roots of inverted repeat *carotenoid cleavage dioxygenase 1* (ir*CCD1*)_45#-related cross plants (at 9 wk post inoculation (wpi)) inoculated with or without (control) *Rhizophagus irregularis* in 2-l pots. (e) Capsule number analyses of ir*CCD1*_45#-related cross plants (at 9 wpi) inoculated with or without (control) *R. irregularis* in 2-l pots. (f, g) Concentrations of 11-carboxyblumenol C-9-O-Glc (f) and AMF-induced lipid TAG 48:2 (g) in roots of ir*CCD1*_48#-related cross plants (at 9 wpi) inoculated with or without (control) *R. irregularis* in 2-l pots. (h) Capsule numbers analyses of ir*CCD1*_48#-related cross plants (at 9 wpi) inoculated with or without (control) *R. irregularis* in 2-l pots. (c–h) Mean ± SD, $n = 8$. Two-way analysis of variance with Tukey's multiple comparisons test: $P < 0.05$. Different letters indicate significant differences between the columns.

plant developmental stage, plant and fungal species involved, the indirect effects of other organisms, and even root metabolomes could affect the outcome of the AMF–host plant relationship (Ronsheim, 2012; Jin *et al.*, 2017; Kaur *et al.*, 2022). We found that *N. attenuata* plants grown in their native habitats and colonized by AMF are much healthier and larger than those grown in the glasshouse (data not shown), and it would be better to investigate the biological functions of blumenol markers on the plant–AMF relationship in the field.

Arbuscular mycorrhizal fungi can use its extraradical hyphae to form underground CMNs that connect neighboring plants (Wipf *et al.*, 2019). In our study, we found that when plants, with different levels of AMF-induced specific lipids, were grown in a competitive environment in the same pot, the lipids levels were similar between the two competing plants (Figs 5d,g, S6b,d). As the lipids are the main nutrients supplied for the fungal growth (Wang *et al.*, 2017), one hypothesis is that lipids are uniformly distributed within the fungal hyphal network connecting

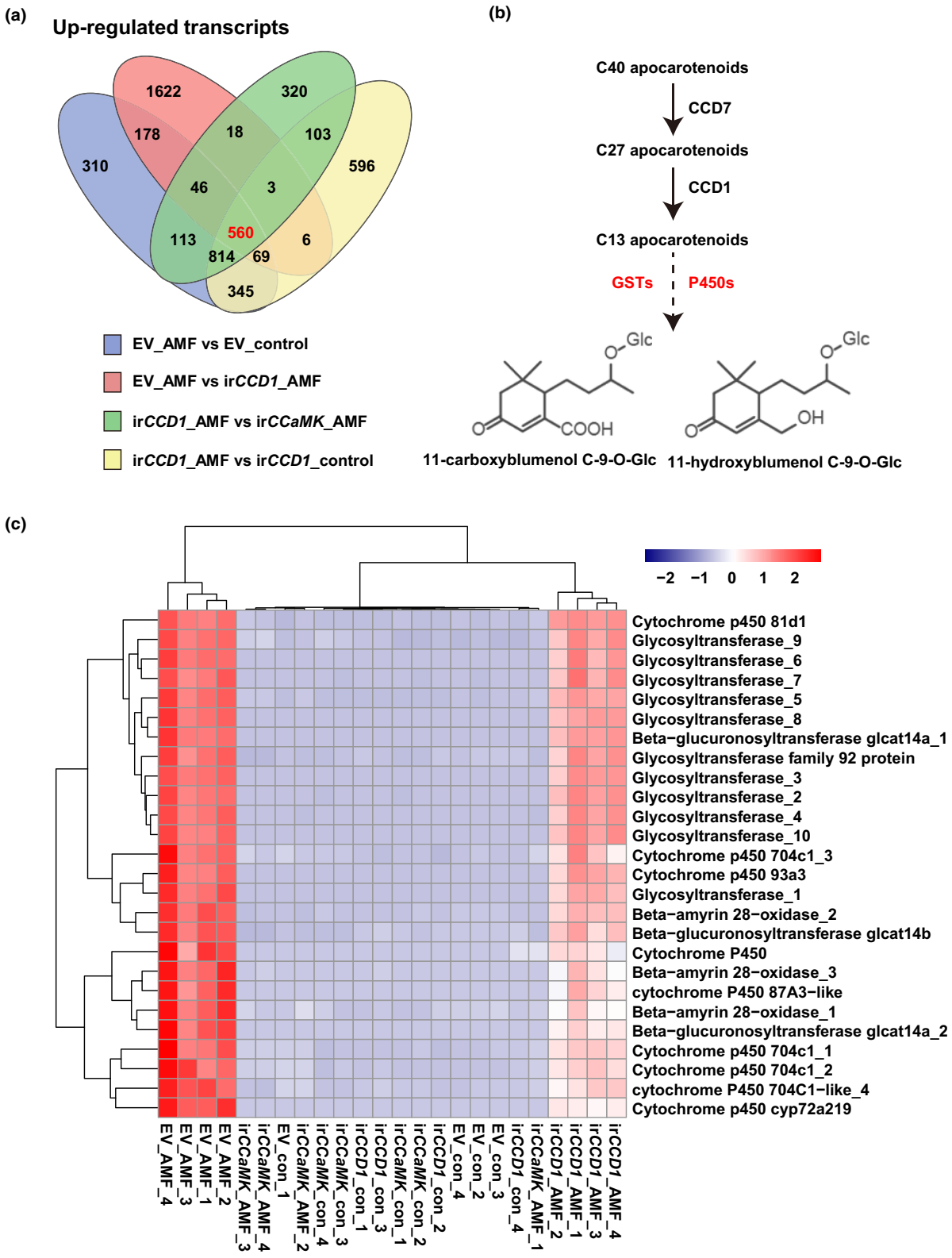

Fig. 6 Candidate enzymes involved in blumenol biosynthesis. (a) Venn diagram analysis identified 560 genes whose expression patterns correlated with blumenol accumulations. Data are from the transcriptome analysis of roots of empty vector (EV), inverted repeat (ir*CCaMK*), and inverted repeat (ir*CCD1*) plants inoculated with (arbuscular mycorrhizal fungi (AMF)) or without (control) *Rhizophagus irregularis*. (b) Schematic diagram of proposed biosynthesis process of 11-carboxyblumenol C-9-O-Glc and 11-hydroxyblumenol C-9-O-Glc. (c) Heat map of expression levels of the glycosyltransferases and cytochrome P450s identified in (a).

different plant roots, similar to the inference that mycorrhiza network function as conduits for the distribution of resources among plants in a community as discussed in a recent review (Figueiredo *et al.*, 2021). Alternatively, there could also be leakage from fungal hyphae and subsequent uptake by neighboring plant roots that would be challenging to distinguish and quantify (Figueiredo *et al.*, 2021). In addition, we found that the blumenol differences between EV and ir*CCD1* plants grown in the same 2-l pots (Figs 5c,f, S6a,c) were smaller than those between EV and ir*CCD1* plants grown in single pots (Fig. 1b). The situation may be similar to the colonization of nonhost plants in the presence of nurse plants in which nutrient and signal transport between host and nonhost plants occurs via CMNs (Wang *et al.*, 2022). There could also be other signals, produced by the EV background plant, and transferred among plants sharing a pot, which recovers the reduced lipid accumulations in ir*CCD1*-background roots. Furthermore, despite very careful root harvesting procedures, we cannot fully rule out the possibility that the root systems of both plants in the same pot had micrografted and were not completely separated, as hypothesized in a previous study (Wang *et al.*, 2018b).

Blumenol markers are synthesized in roots colonized by AMF, and can be transferred to shoots. The pattern is reminiscent of the plant hormone abscisic acid (ABA), which is also a mobile whole-plant signal that regulates numerous aspects of plant growth, development, and stress responses. Abscisic acid is also derived from a C40 carotenoid via oxidative cleavage (Liotenberg *et al.*, 1999) and has a regulatory role in mycorrhizal root colonization. Studies using a mutant defective in ABA biosynthesis demonstrated that ABA promotes arbuscule formation in tomato (*Solanum lycopersicum*; Herrera-Medina *et al.*, 2007; Martín-Rodríguez *et al.*, 2011). Studies in *M. truncatula* demonstrated that ABA has a dual effect on AMF symbiosis: low ABA concentrations promote fungal colonization with the participation of a PROTEIN PHOSPHATASE 2A (PP2A) holoenzyme subunit, while high ABA concentrations impair the colonization (Charpentier *et al.*, 2014). In addition, ABA accumulations are enhanced by AMF colonization under drought conditions (Ruiz-Lozano *et al.*, 2016). Considering that both ABA and blumenols are apocarotenoids and are involved in AMF colonization, and the transport and signaling pathways of ABA have been well-studied (Zhang, 2014), it might be valuable to investigate how blumenol markers are transported and whether there are specific and conserved signaling pathways involved.

Although silencing *CCD1* was a good starting point for investigating the biological functions of blumenols, this target has a number of drawbacks for an analysis of blumenol function, as silencing *CCD1* not only reduces blumenol biosynthesis but also impairs arbuscule maturation (Floss *et al.*, 2008). The last steps in the blumenol biosynthesis would provide a more valuable target for functional studies, as these manipulations are less likely to have pleiotropic effects on the plant–AMF relationship. By combining the RNA-seq data and blumenol accumulation pattern in the roots of EV, ir*CCaMK*, and ir*CCD1*, we identified several *GSTs* and *CYPs* that could catalyze the later-stage glycosylation and hydroxylation/carboxylation steps. Furthermore, using *in vitro* enzymatic assays, we identified one *GST* gene, *GST4*, which is likely involved in the glycosylation of the blumenol markers (Fig. S7c). However, without access to appropriate substrates, and without knowing the order of the catalytic steps, our progress was limited. One alternative way is to use a virus-induced gene silencing (VIGS) strategy to silence the candidate genes and then perform AMF colonization experiments. By quantifying blumenol accumulations in the roots of silenced plants, we could be able to narrow down the list of candidate genes, and generate the related knockdown or knockout transgenic lines to further uncover their roles in the last blumenol–biosynthetic steps. Once verified, these transgenic lines could provide valuable tools for understanding the potential signaling functions of blumenols, and in the identification of other factors that influence the highly context-dependent plant–AMF relationships. Specifically in the context of this work, these transgenic lines would allow for rigorous tests of the hypothesis that these AMF-indicative blumenols function as whole-plant signals coordinating photosynthate flux, first to support the lipid requirements of AMF nutrition in the roots and later, to the shoots, to support seed filling, as plants attain reproductive maturity.

Acknowledgements

We thank Dr Karin Groten for critical review of the manuscript and technical support in AMF colonization analysis. Dr Veit Grabe for microscopic support. Dr Klaus Gase and Wibke Seibt for support in the generation and screening of transgenic plants. Ana Catarina Rocha and Thomas Hahn for technical support for metabolite analysis. Dr Benke Hong for technical support regarding the enzymatic activity assay. This work was supported by the Max Planck Society. Open Access funding enabled and organized by Projekt DEAL.

Competing interests

None declared.

Author contributions

YY and ITB designed the experiments and wrote the paper. YY conducted all glasshouse experiments, and analyzed the data. ITB and GB conducted field experiments. RR helped analyze the raw data of RNA-seq. RH developed the lipid analysis procedure and provided valuable technical support in metabolite analysis. In addition, RR and RH helped to write the Materials and Methods section. All authors provided comments on the manuscript.

ORCID

Gundega Baldwin https://orcid.org/0000-0002-0704-2508
Ian T. Baldwin https://orcid.org/0000-0001-5371-2974
Rayko Halitschke https://orcid.org/0000-0002-1109-8782
Rishav Ray https://orcid.org/0000-0002-9604-3018
Yanrong You https://orcid.org/0000-0002-6175-7993

Data availability

The raw reads of the RNA-seq analysis are deposited in the NCBI Sequence Read Archive (SRA) database under the BioProject accession PRJNA889423. Other data that support the findings of this study are available from the corresponding author upon request.

References

Ablazov A, Mi J, Jamil M, Jia K-P, Wang JY, Feng Q, Al-Babili S. 2020. The apocarotenoid zaxinone is a positive regulator of strigolactone and abscisic acid biosynthesis in Arabidopsis roots. *Frontiers in Plant Science* **11**: 578.

Bago B, Pfeffer PE, Shachar-Hill Y. 2000. Carbon metabolism and transport in arbuscular mycorrhizas. *Plant Physiology* **124**: 949–958.

Baldwin IT, Gorham D, Schmelz EA, Lewandowski CA, Lynds GY. 1998. Allocation of nitrogen to an inducible defense and seed production in *Nicotiana attenuata*. *Oecologia* **115**: 541–552.

Baldwin IT, Morse L. 1994. Up in smoke: II. Germination of *Nicotiana attenuata* in response to smoke-derived cues and nutrients in burned and unburned soils. *Journal of Chemical Ecology* **20**: 2373–2391.

Baldwin IT, Preston C, Euler M, Gorham D. 1997. Patterns and consequences of benzyl acetone floral emissions from *Nicotiana attenuata* plants. *Journal of Chemical Ecology* **23**: 2327–2343.

Baldwin IT, Staszak-Kozinski L, Davidson R. 1994. Up in smoke: I. Smoke-derived germination cues for postfire annual, *Nicotiana attenuata* torr Ex. Watson. *Journal of Chemical Ecology* **20**: 2345–2371.

Bennett AE, Groten K. 2022. The costs and benefits of plant–arbuscular mycorrhizal fungal interactions. *Annual Review of Plant Biology* **73**: 649–672.

Bravo A, Brands M, Wewer V, Dörmann P, Harrison MJ. 2017. Arbuscular mycorrhiza-specific enzymes FatM and RAM 2 fine-tune lipid biosynthesis to promote development of arbuscular mycorrhiza. *New Phytologist* **214**: 1631–1645.

Bravo A, York T, Pumplin N, Mueller LA, Harrison MJ. 2016. Genes conserved for arbuscular mycorrhizal symbiosis identified through phylogenomics. *Nature Plants* **2**: 15208.

Breuillin-Sessoms F, Floss DS, Gomez SK, Pumplin N, Ding Y, Levesque-Tremblay V, Noar RD, Daniels DA, Bravo A, Eaglesham JB. 2015. Suppression of arbuscule degeneration in *Medicago truncatula* phosphate transporter4 mutants is dependent on the ammonium transporter 2 family protein AMT2; 3. *Plant Cell* **27**: 1352–1366.

Bubner B, Gase K, Berger B, Link D, Baldwin IT. 2006. Occurrence of tetraploidy in *Nicotiana attenuata* plants after *Agrobacterium*-mediated transformation is genotype specific but independent of polysomaty of explant tissue. *Plant Cell Reports* **25**: 668–675.

Charpentier M, Sun J, Wen J, Mysore KS, Oldroyd GE. 2014. Abscisic acid promotion of arbuscular mycorrhizal colonization requires a component of the PROTEIN PHOSPHATASE 2A complex. *Plant Physiology* **166**: 2077–2090.

Choi J, Summers W, Paszkowski U. 2018. Mechanisms underlying establishment of arbuscular mycorrhizal symbioses. *Annual Review of Phytopathology* **56**: 135–160.

Das D, Paries M, Hobecker K, Gigl M, Dawid C, Lam H-M, Zhang J, Chen M, Gutjahr C. 2022. PHOSPHATE STARVATION RESPONSE transcription factors enable arbuscular mycorrhiza symbiosis. *Nature Communications* **13**: 477.

Euler M, Baldwin IT. 1996. The chemistry of defense and apparency in the corollas of *Nicotiana attenuata*. *Oecologia* **107**: 102–112.

Felemban A, Braguy J, Zurbriggen MD, Al-Babili S. 2019. Apocarotenoids involved in plant development and stress response. *Frontiers in Plant Science* **10**: 1168.

Figueiredo AF, Boy J, Guggenberger G. 2021. Common mycorrhizae network: a review of the theories and mechanisms behind underground interactions. *Frontiers in Fungal Biology* **2**: 735299.

Fiorilli V, Wang JY, Bonfante P, Lanfranco L, Al-Babili S. 2019. Apocarotenoids: old and new mediators of the arbuscular mycorrhizal symbiosis. *Frontiers in Plant Science* **10**: 1186.

Floss DS, Schliemann W, Schmidt J, Strack D, Walter MH. 2008. RNA interference-mediated repression of *MtCCD1* in mycorrhizal roots of *Medicago truncatula* causes accumulation of C_{27} apocarotenoids, shedding light on the functional role of CCD1. *Plant Physiology* **148**: 1267–1282.

Gase K, Weinhold A, Bozorov T, Schuck S, Baldwin IT. 2011. Efficient screening of transgenic plant lines for ecological research. *Molecular Ecology Resources* **11**: 890–902.

Gaude N, Bortfeld S, Duensing N, Lohse M, Krajinski F. 2012. Arbuscule-containing and non-colonized cortical cells of mycorrhizal roots undergo extensive and specific reprogramming during arbuscular mycorrhizal development. *The Plant Journal* **69**: 510–528.

Glawe GA, Zavala JA, Kessler A, Van Dam NM, Baldwin IT. 2003. Ecological costs and benefits correlated with trypsin protease inhibitor production in *Nicotiana attenuata*. *Ecology* **84**: 79–90.

Groten K, Nawaz A, Nguyen NH, Santhanam R, Baldwin IT. 2015. Silencing a key gene of the common symbiosis pathway in *Nicotiana attenuata* specifically impairs arbuscular mycorrhizal infection without influencing the root-associated microbiome or plant growth. *Plant, Cell & Environment* **38**: 2398–2416.

Gutjahr C, Parniske M. 2013. Cell and developmental biology of arbuscular mycorrhiza symbiosis. *Annual Review of Cell and Developmental Biology* **29**: 593–617.

He J, Fandino RA, Halitschke R, Luck K, Köllner TG, Murdock MH, Ray R, Gase K, Knaden M, Baldwin IT. 2019. An unbiased approach elucidates variation in (*S*)-(+)-linalool, a context-specific mediator of a tri-trophic interaction in wild tobacco. *Proceedings of the National Academy of Sciences, USA* **116**: 14651–14660.

Herrera-Medina MJ, Steinkellner S, Vierheilig H, Ocampo Bote JA, Garcia Garrido JM. 2007. Abscisic acid determines arbuscule development and functionality in the tomato arbuscular mycorrhiza. *New Phytologist* **175**: 554–564.

Hou X, Rivers J, León P, McQuinn RP, Pogson BJ. 2016. Synthesis and function of apocarotenoid signals in plants. *Trends in Plant Science* **21**: 792–803.

Javot H, Penmetsa RV, Terzaghi N, Cook DR, Harrison MJ. 2007. A *Medicago truncatula* phosphate transporter indispensable for the arbuscular mycorrhizal symbiosis. *Proceedings of the National Academy of Sciences, USA* **104**: 1720–1725.

Jiang Y, Wang W, Xie Q, Liu N, Liu L, Wang D, Zhang X, Yang C, Chen X, Tang D. 2017. Plants transfer lipids to sustain colonization by mutualistic mycorrhizal and parasitic fungi. *Science* **356**: 1172–1175.

Jin L, Wang Q, Wang Q, Wang X, Gange AC. 2017. Mycorrhizal-induced growth depression in plants. *Symbiosis* **72**: 81–88.

Johnson NC, Graham JH, Smith FA. 1997. Functioning of mycorrhizal associations along the mutualism–parasitism continuum. *New Phytologist* **135**: 575–585.

Johnson NC, Wilson GW, Bowker MA, Wilson JA, Miller RM. 2010. Resource limitation is a driver of local adaptation in mycorrhizal symbioses. *Proceedings of the National Academy of Sciences, USA* **107**: 2093–2098.

Kaur S, Campbell BJ, Suseela V. 2022. Root metabolome of plant–arbuscular mycorrhizal symbiosis mirrors the mutualistic or parasitic mycorrhizal phenotype. *New Phytologist* **234**: 672–687.

Keymer A, Gutjahr C. 2018. Cross-kingdom lipid transfer in arbuscular mycorrhiza symbiosis and beyond. *Current Opinion in Plant Biology* **44**: 137–144.

Keymer A, Pimprikar P, Wewer V, Huber C, Brands M, Bucerius SL, Delaux P-M, Klingl V, von Roepenack-Lahaye E, Wang TL. 2017. Lipid transfer from plants to arbuscular mycorrhiza fungi. *eLife* **6**: e29107.

Ko MR, Song M-H, Kim JK, Baek S-A, You MK, Lim S-H, Ha S-H. 2018. RNAi-mediated suppression of three carotenoid-cleavage dioxygenase genes, *OsCCD1*, *4a*, and *4b*, increases carotenoid content in rice. *Journal of Experimental Botany* **69**: 5105–5116.

Krügel T, Lim M, Gase K, Halitschke R, Baldwin IT. 2002. *Agrobacterium*-mediated transformation of *Nicotiana attenuata*, a model ecological expression system. *Chemoecology* **12**: 177–183.

Lendenmann M, Thonar C, Barnard RL, Salmon Y, Werner RA, Frossard E, Jansa J. 2011. Symbiont identity matters: carbon and phosphorus fluxes

between *Medicago truncatula* and different arbuscular mycorrhizal fungi. *Mycorrhiza* **21**: 689–702.

Li S, Joo Y, Cao D, Li R, Lee G, Halitschke R, Baldwin G, Baldwin IT, Wang M. 2020. Strigolactone signaling regulates specialized metabolism in tobacco stems and interactions with stem-feeding herbivores. *PLoS Biology* **18**: e3000830.

Liotenberg S, North H, Marion-Poll A. 1999. Molecular biology and regulation of abscisic acid biosynthesis in plants. *Plant Physiology and Biochemistry* **37**: 341–350.

Luginbuehl LH, Menard GN, Kurup S, Van Erp H, Radhakrishnan GV, Breakspear A, Oldroyd GE, Eastmond PJ. 2017. Fatty acids in arbuscular mycorrhizal fungi are synthesized by the host plant. *Science* **356**: 1175–1178.

Martín-Rodríguez JÁ, León-Morcillo R, Vierheilig H, Ocampo JA, Ludwig-Müller J, García-Garrido JM. 2011. Ethylene-dependent/ethylene-independent ABA regulation of tomato plants colonized by arbuscular mycorrhiza fungi. *New Phytologist* **190**: 193–205.

Mitra S, Baldwin IT. 2008. Independently silencing two photosynthetic proteins in *Nicotiana attenuata* has different effects on herbivore resistance. *Plant Physiology* **148**: 1128–1138.

Moreno JC, Mi J, Alagoz Y, Al-Babili S. 2021. Plant apocarotenoids: from retrograde signaling to interspecific communication. *The Plant Journal* **105**: 351–375.

Müller LM, Harrison MJ. 2019. Phytohormones, miRNAs, and peptide signals integrate plant phosphorus status with arbuscular mycorrhizal symbiosis. *Current Opinion in Plant Biology* **50**: 132–139.

Nadal M, Sawers R, Naseem S, Bassin B, Kulicke C, Sharman A, An G, An K, Ahern KR, Romag A. 2017. An *N*-acetylglucosamine transporter required for arbuscular mycorrhizal symbioses in rice and maize. *Nature Plants* **3**: 1–7.

Nouri E, Breuillin-Sessoms F, Feller U, Reinhardt D. 2014. Phosphorus and nitrogen regulate arbuscular mycorrhizal symbiosis in *Petunia hybrida*. *PLoS ONE* **9**: e90841.

Nouri E, Surve R, Bapaume L, Stumpe M, Chen M, Zhang Y, Ruyter-Spira C, Bouwmeester H, Glauser G, Bruisson S. 2021. Phosphate suppression of arbuscular mycorrhizal symbiosis involves gibberellic acid signaling. *Plant and Cell Physiology* **62**: 959–970.

Riedel T, Groten K, Baldwin IT. 2008. Symbiosis between *Nicotiana attenuata* and *Glomus intraradices*: ethylene plays a role, jasmonic acid does not. *Plant, Cell & Environment* **31**: 1203–1213.

Ronsheim ML. 2012. The effect of mycorrhizae on plant growth and reproduction varies with soil phosphorus and developmental stage. *The American Midland Naturalist* **167**: 28–39.

Roth R, Paszkowski U. 2017. Plant carbon nourishment of arbuscular mycorrhizal fungi. *Current Opinion in Plant Biology* **39**: 50–56.

Ruiz-Lozano JM, Aroca R, Zamarreño ÁM, Molina S, Andreo-Jiménez B, Porcel R, García-Mina JM, Ruyter-Spira C, López-Ráez JA. 2016. Arbuscular mycorrhizal symbiosis induces strigolactone biosynthesis under drought and improves drought tolerance in lettuce and tomato. *Plant, Cell & Environment* **39**: 441–452.

Salem MA, Jüppner J, Bajdzienko K, Giavalisco P. 2016. Protocol: a fast, comprehensive and reproducible one-step extraction method for the rapid preparation of polar and semi-polar metabolites, lipids, proteins, starch and cell wall polymers from a single sample. *Plant Methods* **12**: 45.

Schwachtje J, Minchin PE, Jahnke S, van Dongen JT, Schittko U, Baldwin IT. 2006. SNF1-related kinases allow plants to tolerate herbivory by allocating carbon to roots. *Proceedings of the National Academy of Sciences, USA* **103**: 12935–12940.

Schwartz SH, Qin X, Zeevaart JD. 2001. Characterization of a novel carotenoid cleavage dioxygenase from plants. *Journal of Biological Chemistry* **276**: 25208–25211.

Shi J, Zhao B, Zheng S, Zhang X, Wang X, Dong W, Xie Q, Wang G, Xiao Y, Chen F. 2021. A phosphate starvation response-centered network regulates mycorrhizal symbiosis. *Cell* **184**: 5527–5540.

Simkin AJ, Schwartz SH, Auldridge M, Taylor MG, Klee HJ. 2004. The tomato *carotenoid cleavage dioxygenase 1* genes contribute to the formation of the flavor volatiles β-ionone, pseudoionone, and geranylacetone. *The Plant Journal* **40**: 882–892.

Smith SE, Read DJ. 2008. *Mycorrhizal symbiosis*. Cambridge, UK: Academic Press.

Song Y, Wang M, Zeng R, Groten K, Baldwin IT. 2019. Priming and filtering of antiherbivore defences among *Nicotiana attenuata* plants connected by mycorrhizal networks. *Plant, Cell & Environment* **42**: 2945–2961.

Spatafora JW, Chang Y, Benny GL, Lazarus K, Smith ME, Berbee ML, Bonito G, Corradi N, Grigoriev I, Gryganskyi A. 2016. A phylum-level phylogenetic classification of zygomycete fungi based on genome-scale data. *Mycologia* **108**: 1028–1046.

Sun Z, Hans J, Walter MH, Matusova R, Beekwilder J, Verstappen FW, Ming Z, van Echtelt E, Strack D, Bisseling T. 2008. Cloning and characterisation of a maize carotenoid cleavage dioxygenase (*ZmCCD1*) and its involvement in the biosynthesis of apocarotenoids with various roles in mutualistic and parasitic interactions. *Planta* **228**: 789–801.

Votta C, Fiorilli V, Haider I, Wang JY, Balestrini R, Petřík I, Tarkowská D, Novák O, Serikbayeva A, Bonfante P. 2022. Zaxinone synthase controls arbuscular mycorrhizal colonization level in rice. *The Plant Journal* **111**: 1688–1700.

Wang JY, Haider I, Jamil M, Fiorilli V, Saito Y, Mi J, Baz L, Kountche BA, Jia K-P, Guo X. 2019. The apocarotenoid metabolite zaxinone regulates growth and strigolactone biosynthesis in rice. *Nature Communications* **10**: 810.

Wang M, Schäfer M, Li D, Halitschke R, Dong C, McGale E, Paetz C, Song Y, Li S, Dong J *et al.* 2018a. Blumenols as shoot markers of root symbiosis with arbuscular mycorrhizal fungi. *eLife* **7**: e37093.

Wang M, Wilde J, Baldwin IT, Groten K. 2018b. *Nicotiana attenuata*'s capacity to interact with arbuscular mycorrhiza alters its competitive ability and elicits major changes in the leaf transcriptome. *Journal of Integrative Plant Biology* **60**: 242–261.

Wang W, Shi J, Xie Q, Jiang Y, Yu N, Wang E. 2017. Nutrient exchange and regulation in arbuscular mycorrhizal symbiosis. *Molecular Plant* **10**: 1147–1158.

Wang Y, He X, Yu F. 2022. Non-host plants: are they mycorrhizal networks players? *Plant Diversity* **44**: 127–134.

Wewer V, Brands M, Dörmann P. 2014. Fatty acid synthesis and lipid metabolism in the obligate biotrophic fungus *Rhizophagus irregularis* during mycorrhization of *Lotus japonicus*. *The Plant Journal* **79**: 398–412.

Wipf D, Krajinski F, van Tuinen D, Recorbet G, Courty PE. 2019. Trading on the arbuscular mycorrhiza market: from arbuscules to common mycorrhizal networks. *New Phytologist* **223**: 1127–1142.

Zhang D-P. 2014. *Abscisic acid: metabolism, transport and signaling*. New York, NY, USA: Springer.

Supporting Information

Additional Supporting Information may be found online in the Supporting Information section at the end of the article.

Dataset S1 RNA-seq analysis of genes upregulated by arbuscular mycorrhizal fungi (AMF) and *carotenoid cleavage dioxygenase 1* (*CCD1*).

Dataset S2 RNA-seq analysis of genes likely involved in blumenol biosynthesis.

Fig. S1 Characterization of ir*CCD1* transgenic lines.

Fig. S2 RNA-seq analysis.

Fig. S3 Lipid analysis of empty vector (EV) and ir*CCD1*_#45 plants grown in the field.

Fig. S4 Transcript abundances of strigolactone biosynthesis genes *CCD7* and *CCD8*, and abscisic acid concentrations.

Fig. S5 Blumenols are positively correlated with arbuscular mycorrhizal fungi (AMF)-induced lipids in singly grown plants.

Fig. S6 Blumenol and lipid levels in the ir*CCD1*_#45- and ir*CCD1*_#48-related cross plants.

Fig. S7 Candidate enzymes involved in blumenol biosynthesis.

Methods S1 RNA sequencing, *in vitro* enzymatic activity assays and gene accession numbers.

Table S1 Primers used in this study.

Please note: Wiley is not responsible for the content or functionality of any Supporting Information supplied by the authors. Any queries (other than missing material) should be directed to the *New Phytologist* Central Office.